Journal of Magnetism and Magnetic Materials 422 (2017) 287–298

Contents lists available at ScienceDirect

Journal of Magnetism and Magnetic Materials

journal homepage: www.elsevier.com/locate/jmmm

Thermoelectric properties of $TbFe_2$ and $TbCo_2$ in C15- laves phase: Spin-polarized DFT+U approach

A.H. Reshak [a,b,*]

[a] New Technologies - Research Centre, University of West Bohemia, Univerzitni 8, Pilsen 306 14, Czech Republic
[b] School of Material Engineering, University Malaysia Perlis, Kangar, Perlis 01007, Malaysia

ARTICLE INFO

Article history:
Received 4 June 2016
Received in revised form
3 September 2016
Accepted 5 September 2016
Available online 6 September 2016

Keywords:
Spin-polarization
Transport properties
Electronic materials

ABSTRACT

Thermoelectric properties of materials are intimately related to their electronic band structure. Combining first- and second-principles calculations, we have obtained the transport properties for the spin-up and spin-down electrons of the laves phase $TbFe_2$ and $TbCo_2$ compounds. The unique band structure feature and the density of states at Fermi level (E_F) promote the E_F to a point where carriers are in energetic proximity to these features. The non-zero density of states at E_F for the spin-up (↑) and spin-down (↓) electrons leads to unusual transport properties because both the (↑) and (↓) densities contributes to the states at E_F. The parabolic bands in the vicinity of E_F enhance the carriers mobility and hence the transport properties of $TbFe_2$ and $TbCo_2$. Calculations show that the spin-up/down transport coefficients are temperature-dependent. It has been found that $TbCo_2$ possess larger Seebeck coefficient than that of $TbFe_2$ and hence the power factor. The calculated Seebeck coefficient of $TbCo_2$ agree well with the available experimental data.

1. Introduction

In strongly correlated electron systems, various interesting phenomena are caused by the effect of strong Coulomb repulsions. The cubic Laves phase intermetallic compounds REX_2 (where RE-=rare earth elements and X=transition metal) have attracted much attention because of unusual metamagnetic transitions which originate from the coexistence and interaction of magnetic moments of highly localized RE 4*f* electrons and itinerant 3*d* electrons of the X [1,2]. REX_2 ($TbFe_2$ and $TbCo_2$) crystallizes in a cubic $MgCu_2$ type structure in which RE and X atoms occupy one equivalent site in each sublattice [3]. The extremely large discontinuity observed in the Seebeck coefficient or thermopower (S) and electrical resistivity in connection with first-order magnetic transitions in $DyCo_2$, $HoCo_2$ and $ErCo_2$ was investigated under the assumption that the Fermi energy (E_F) is situated in a steep decrease of the 3*d* band and this situation is responsible for the appearance of the first-order transition [4]. The calculated variation of the density of states at E_F in the isostructurally related compounds for instance YFe_2, YCo_2 and YNi_2 [5] support the idea regarding the density of states at E_F in the magnetic $RECo_2$ compounds. It has been found that in $RECo_2$ a similar situation exists above T_c as in the YCo_2 compound. It was stated that the existence of the magnetic RE moments can leads to a first-order transition from a magnetic state to a paramagnetic state by heating the sample [4]. Gratz et al. [4] have reported that the contribution to the Seebeck coefficient caused by the disordered localized 4*f* moments is temperature independent in the range $T > T_c$. In $REFe_2$ compounds the Fe atoms possess an intrinsic magnetic moment and the magnitude of this moment and the related ground state properties are significantly influenced by using different RE atoms [4]. Similarly, using different RE atoms in $RECo_2$ compounds cause pronounced influence on the magnetic behavior of Co atoms and the other ground state properties including the density of states at E_F and hence the transport properties. Gratz et al. [6] have investigated the physical properties of RCo_2 Laves phases, they state that the outstanding magnetic features of the RCo_2 intermetallics are intimately related to the position of the E_F, which is near to a local peak in the density of states.

As the above mentioned compounds have non-zero density of states at Fermi level for the spin-up and spin-down configurations therefore, it is of great interest to investigate the influences of spin fluctuations on the transport properties because the non-zero density of states at E_F leads to unusual transport properties, make these compounds as promising candidates for materials used in spin voltage generators. Therefore, we have addressed ourselves to investigate the transport properties of $TbFe_2$ and $TbCo_2$.

* Corresponding author at: New Technologies - Research Centre, University of West Bohemia, Univerzitni 8, 306 14 Pilsen, Czech Republic.
E-mail address: maalidph@yahoo.co.uk

http://dx.doi.org/10.1016/j.jmmm.2016.09.037
0304-8853/

2. Details of calculations

The $TbCo_2$ and $TbFe_2$ Laves phase crystallizes in cubic symmetry with Fd-3m space group [7–9]. The experimental lattice constants a=7.40 Å for $TbFe_2$ [8,9] and a=5.0932 Å for $TbCo_2$ [7] were optimized by using the full-potential linear augmented plane wave plus the local orbitals (FPLAPW+lo) method as implemented in WIEN2k code [10] within Perdew-Burke-Ernzerhof generalized gradient approximation (PBE-GGA) [11]. The resulting lattice constants are a=7.021 Å for $TbFe_2$ and a=5.056 Å for $TbCo_2$. For the oxides and other highly correlated compounds, were in these systems the electrons are highly localized, the local density approximation (LDA) and the generalized gradient approximation (GGA) are known to fail to give the correct ground state. Therefore, the Coulomb repulsion between the electrons in open shells should be taken into account. It is well known that there is no exchange correlation functional that can include this in an orbital independent way, thus a simpler approach is to add the Hubbard-like on-site repulsion to the Kohn-Sham Hamiltonian. This approach is known as DFT+U. There are different ways in which this can be implemented. In the present work, we have used the method of Anisimov et al. [12] and Liechtenstein et al. [13] where the Coulomb (U) and exchange (J) parameters are used. From the obtained relaxed geometry the ground state properties were determined using the FPLAPW+lo method [11,14,15] within GGA+U (U-Hubbard Hamiltonian). We applied U on the 3*d* orbital of Fe, Co atoms and 4*f* orbital of Tb atoms, we have testify several U values till we reach the satisfactory values that agree well with the previous results [4,7–9]. The U values used here are 0.605, 0.504 and 0.436 Ry for Tb, Co and Fe, respectively.

The calculation of the transport properties of $TbFe_2$ and $TbCo_2$ in C15- Laves phase were performed based on the calculated spin-polarized electronic band structures utilizing the semi-classical Boltzmann theory [16]. Simulations of the transport properties is transition from first- to second-principles methods. The first-principles method used here is all-electron full-potential linear augmented plane wave method whereas the second-principles is BoltzTraP code [16], which solves the semi-classical Bloch-Boltzmann transport equations [16]. The transport properties were obtained from the ground state within the limits of Boltzmann theory [17–19] and the constant relaxation time approximation as implemented in the BoltzTraP code [16]. In short, BoltzTraP performs a Fourier expansion of the quantum chemical band energies. This allows to obtain the electronic group velocity v and inverse mass tensor, as the first and second derivatives of the bands with respect to k. Applying v and to the semiclassical Boltzmann equations, the transport tensors can be evaluated.

In FPLAPW+lo method the potential for the construction of the basis functions inside the sphere of the muffin-tin was spherically symmetric, whereas it was constant outside the sphere [10]. In this calculation the self-consistency is obtained using 1000 $\vec{k}$ points in the irreducible Brillouin zone (*IBZ*). The self-consistent calculations are converged since the total energy of the system is stable within 0.00001 Ry. The calculation of the spin-polarized electronic band structure and the transport properties of $TbFe_2$ and $TbCo_2$ compounds were performed within 30,000 $\vec{k}$ points in the *IBZ* as the accurate calculations of transport properties of metals require the dense sampling of the Brillouin zone. It is well known that first-principles calculations are a powerful and useful tool to predict the crystal structure and its properties related to the electron configuration of a material before its synthesis [20,21]. It is worth to notice, that the predictive power of first-principles quantum electronic structure calculations due to increased speed of computers and recent development of new and powerful computational methods nowadays allows for the rational design on paper of new materials for technology applications. One good example is the recent prediction of the average battery voltage for a 5 V lithium-ion battery by Eglitis and Borstel [22,23].

3. Results and discussion

3.1. Salient features of the spin-polarized electronic band structure

To explore the band dispersion, we have calculated spin-polarized electronic band structure of $TbFe_2$ and $TbCo_2$ for spin-up (↑) and spin-down (↓) electrons. These are shown in Fig. 1(a–d). It has been found that from the calculated spin-polarized electronic band structure and density of states, the spin-up/down exhibit metallic structure with a density of states at E_F, $N(E_F)$, of about 1.144 (3.904) (state/eV/unit cell) for spin-up (spin-down) of $TbFe_2$ whereas it is about 3.750 (14.984) (state/eV/unit cell) for spin-up (spin-down) of $TbCo_2$. The calculated bare electronic specific heat coefficient (γ) is about 0.198 (0.677) mJ/(mol cell K^2) for spin-up (spin-down) of $TbFe_2$ while it is about 0.650 (2.599) mJ/(mol cell K^2) for spin-up (spin-down) of $TbCo_2$. It is well-known that the density of states at E_F, $N(E_F)$ leads to unusual transport properties because both the spin-up and spin-down densities contributes to the states at E_F. Similar behavior was observed in Co_2MnAl and Co_2MnSn compounds [24]. Therefore, the bands which cross E_F are responsible for the transport properties of the compound and those bands which are not crossing E_F will contribute negligibly small to the transport properties [25]. Calculations of the density of states for $TbFe_2$ and $TbCo_2$ revealed the importance of the 3*d*–4*d* hybridization in forming the *d* band structure of these Laves phases. According to these calculations, the Fermi level lies near a sharp peak in the density of states caused mainly by the 3*d* states.

In addition, we have calculated the Fermi surface of the spin-up/down for $TbFe_2$ and $TbCo_2$ compounds as shown in Fig. 2(a,c,e, g). It is clear that Fermi surface consist of white regions which represent the holes concentration and colored regions which indicates the presence of electrons [26]. These colors give an idea about the speed of electrons for instance the red color represent the highest speed, yellow green and blue have intermediate speed whereas the violet color show lowest speed. The colors of Fermi surface confirms that replacing Fe by Co cause reduce/increase the speed of the electrons at Fermi surface. Usually the transport properties is related to the electrons in the system, and these electrons are defined through Fermi surface, which determine the electrical conductivity [26].

The electronic band structure for (↑) and (↓) in the area around E_F show that there exists a parabolic bands in the vicinity of Fermi level (Fig. 1a–d and Fig. 2b,d,f,h). This implies that the $TbFe_2$ and $TbCo_2$ shows highest **k**- dispersion bands around E_F and thus lowest effect masses and hence the highest mobility carriers. Therefore, we have calculated the effective mass of electrons (m_e^*) for spin-up and spin-down of $TbFe_2$ and $TbCo_2$. Usually we estimated the value of effective mass of electrons from the conduction band minimum curvature. The diagonal elements of the effective mass tensor, m_e^*, for the electrons in the conduction band are calculated following this expression;

$$\frac{1}{m_e^*} = \frac{\partial^2 E(k)}{\hbar^2 \partial k^2} \tag{1}$$

The effective mass of electron is assessed by fitting the electronic band structure to a parabolic function Eq. (1). The calculated electron effective mass ratio (m_e^*/m_e) around Γ point of BZ is about 0.0240 (0.0327) for spin-up configuration of $TbFe_2$ ($TbCo_2$), while it is 0.0094 (0.0099) for spin-down configuration of $TbFe_2$ ($TbCo_2$). Therefore, the spin-up electrons of both compounds possess

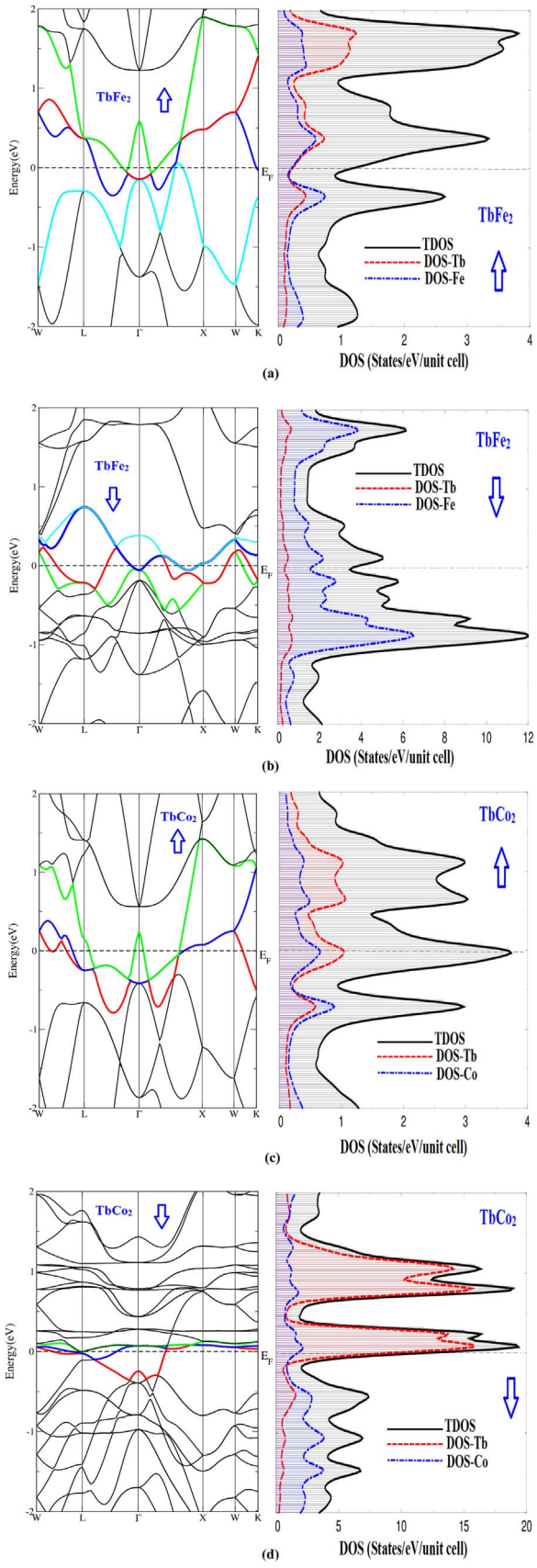

Fig. 1. Calculated spin-polarized electronic band structure and density of states; (a) For (↑) electrons of $TbFe_2$; (b) For (↓) electrons of $TbFe_2$; (c) For (↑) electrons of $TbCo_2$; (d) For (↓) electrons of $TbCo_2$.

higher mobility than that of spin-down.

3.2. Transport properties

3.2.1. Charge carriers concentration and electrical conductivity

We have investigated the carriers concentration of $TbFe_2$ and $TbCo_2$ for (↑) and (↓) at three constant temperatures (300, 600 and 900) K at the chemical potential $\mu - E_F = \pm 0.15$ eV in the vicinity of Fermi level as shown in Fig. 2(b,d,f,h). It has been noticed that the difference between chemical potential and Fermi energy $(\mu - E_F)$ is positive for valence bands and negative for conduction bands. It is clear from the electronic band structure (Fig. 1a–d and Fig. 2b,d,f,h) that $TbFe_2$ and $TbCo_2$ have parabolic bands in the vicinity of Fermi level therefore, the carriers exhibit low effective mass and hence high mobility. It has been found that the investigated materials exhibit a maximum carriers concentration and n-/p-type conductions in the vicinity of Fermi level.

To support this statement the temperature dependent carriers concentration of $TbFe_2$ and $TbCo_2$ for the spin-up/down electrons at a certain value of the chemical potential ($\mu = E_F$) were investigated. It has been noticed that the carriers concentration of the spin-up (↑) electrons of both compounds exhibits n-type conductions as shown in Fig. 3(a,b). The carriers concentration of (↑) $TbFe_2$ show a value of about -22.5 e/uc at 50 K which reaches to -22.56 e/uc at 900 K. Whereas for (↑) $TbCo_2$ it is about -20.48 e/ucat 50 K and -20.405 e/uc at 900 K. Fig. 3(c,d) illustrated the carriers concentration of the spin-down (↓) electrons which represent the p-type conductions. For the spin-up (↓) electrons of $TbFe_2$ and the maximum value 22.5 e/uc is achieved at about 50 K. A significant reduction in the carriers concentration occurs with increasing the temperature up to 600 K then it shows almost stable value. While for the spin-up (↓) electrons of $TbCo_2$ the maximum value of about 22.5 e/uc is achieved at 50 K which significantly reduces with increasing the temperature to reach 19.0 e/uc at 900 K.

The total carrier concentration is defined as the difference between the hole and the electron concentrations. As it was mentioned above that the spin-up electrons of $TbFe_2$ and $TbCo_2$ possess higher mobility /low effective mass than that of spin-down. Therefore, the calculated total carrier concentration of $TbCo_2$ is ten times higher than that of $TbFe_2$ as shown in Fig. 3(e,f). The calculated total carrier concentration show that the n-type conductions are the dominant.

Usually to gain high thermoelectric efficiency from a cretin material, it is necessary that the investigated material possess high electrical conductivity, large Seebeck coefficient and low thermal conductivity [27]. Therefore, to achieve the highest electrical conductivity, high mobility carriers is required. To achieve this, a material with small effective masses is needed. The electrical conductivity ($\sigma = ne\eta$) is directly proportional to the charge carriers density (n) and their mobility (η) where ($\eta_e = e\tau_e/m_e^*$ and $\eta_h = p\tau_h/m_h^*$) therefore, materials with small effective masses posses high mobility. To achieve the highest electrical conductivity, one need to maintain the charge carriers density and their mobility. We have investigated the electrical conductivity of $TbFe_2$ and $TbCo_2$ for spin-up/down as a function of temperature at a certain value of chemical potential ($\mu = E_F$). Fig. 4(a–d) represents the temperature variation of spin-up (↑) and spin-down (↓) σ/τ. For the spin-up/down electrons of $TbFe_2$ the electrical conductivity increases with increasing the temperature. This is not the case for (↑) (↓) electrons of $TbCo_2$, it has been noticed that for (↑) the electrical conductivity decreases with the temperature, while for (↓) it increases to reach the maximum value at 200 K then drop to the minimum value at 900 K.

The total electrical conductivity is calculated by using two current model [28,29]. It is clear that the total electrical

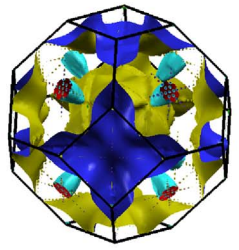

(a)

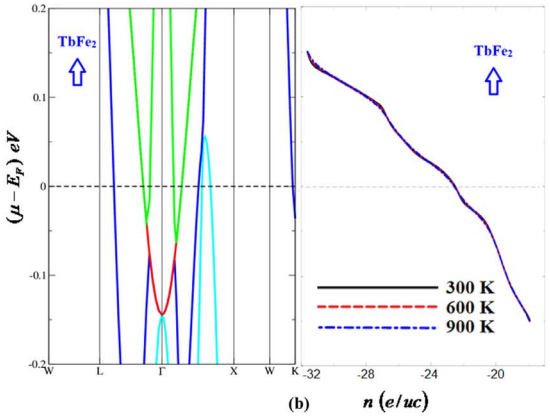
TbFe2
TbFe2
(μ − Ep) eV
W L Γ X W K
-32 -28 -24 -20
300 K
600 K
900 K
n (e/uc)

(b)

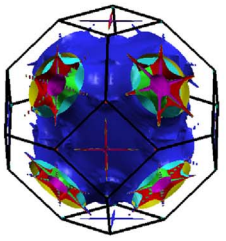

(c)

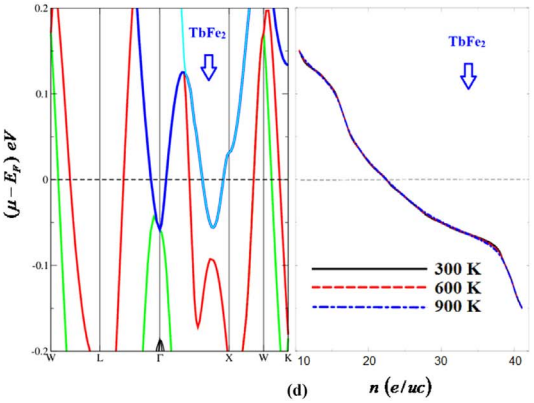
TbFe2
TbFe2
(μ − Ep) eV
W L Γ X W K
10 20 30 40
300 K
600 K
900 K
n (e/uc)

(d)

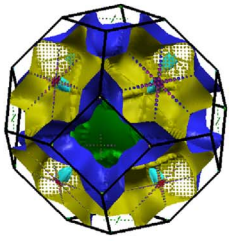

(e)

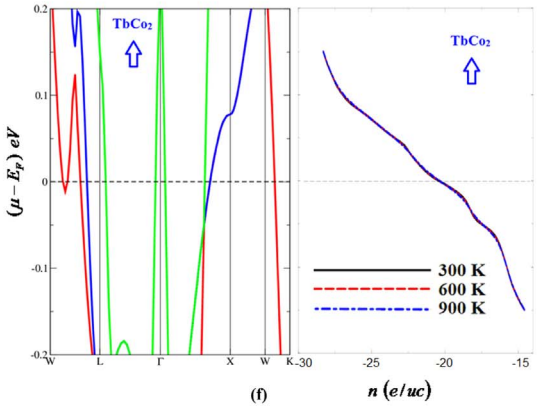
TbCo2
TbCo2
(μ − Ep) eV
W L Γ X W K
-30 -25 -20 -15
300 K
600 K
900 K
n (e/uc)

(f)

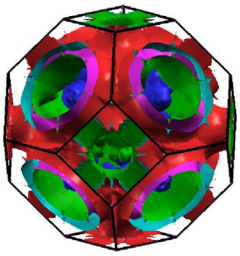

(g)

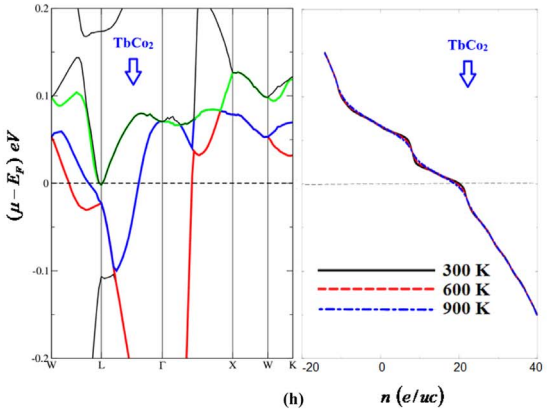
TbCo2
TbCo2
(μ − Ep) eV
W L Γ X W K
-20 0 20 40
300 K
600 K
900 K
n (e/uc)

(h)

conductivity of $TbFe_2$ (Fig. 4e) shows a slight deviation from the linear temperature dependence and the maximum value of about $4.18 \times 10^{20}\,(\Omega ms)^{-1}$ was shown at 900 K, whereas the total electrical conductivity of $TbCo_2$ (Fig. 4f) decreases with increasing the temperature and a maximum value of about $5.1 \times 10^{20}\,(\Omega ms)^{-1}$ was shown at 50 K. Therefore, at a certain value of the chemical potential the carriers concentration and electrical conductivity are temperature-dependent.

To ascertain that the investigated compounds expected to give maximum efficiency in the vicinity of E_F, we have calculated the electrical conductivity of $TbFe_2$ and $TbCo_2$ for (↑)(↓) electrons as a function of chemical potential ($\mu - E_F = \pm 0.15$ eV) at three constant temperatures (300, 600 and 900) K as shown in Fig. 5(a–d). For the (↑) electrons of $TbFe_2$ it is clear that just above and below E_F a significant increases in the electrical conductivity occurs to reach the maximum value of about $3.86 \times 10^{20}\,(\Omega ms)^{-1}$ at 300 K for $\mu - E_F = -0.12$ eV for n-type conductions, and 4.16×10^{20} at 300 K for $\mu - E_F = +0.05$ eV for p-type conductions. While for the (↓) electrons of $TbFe_2$ a maximum value of about $2.63 \times 10^{20}\,(\Omega ms)^{-1}$ was achieved at 300 K and $\mu - E_F = -0.14$ eV for n-type conductions, and about $3.14 \times 10^{20}\,(\Omega ms)^{-1}$ at 300 K and $\mu - E_F = +0.11$ eV for p-type conductions. Whereas for the (↑) electrons of $TbCo_2$ the maximum electrical conductivity of about $4.12 \times 10^{20}\,(\Omega ms)^{-1}$ $(5.21 \times 10^{20}\,(\Omega ms)^{-1})$ for n-type (*p*-type) conductions is achieved at 300 K and $\mu - E_F = -0.14$ eV ($\mu - E_F = +0.07$ eV). While for the (↓) electrons of $TbCo_2$ a maximum electrical conductivity of about $3.96 \times 10^{20}\,(\Omega ms)^{-1}$ $(2.33 \times 10^{20}\,(\Omega ms)^{-1})$ for n-type (*p*-type) conductions is achieved at 300 K and $\mu - E_F = -0.08$ eV ($\mu - E_F = +0.12$ eV).

From above we can conclude that the differences in the electrical conductivity between $TbFe_2$ and $TbCo_2$ for both (↑)(↓) is attributed to the fact that these compounds possess different density of states at E_F, effective masses and Fermi surfaces.

3.2.2. Electronic thermal conductivity

In general the thermal conductivity (κ) consist of two parts, the first part is the electronic contribution κ_e (electrons and holes transporting heat) and second part is the phonon contribution κ_l (phonons traveling through the lattice). We should emphasize that BoltzTraP code calculates only the electronic part κ_e [16]. The electronic thermal conductivity (κ_e/τ) of $TbFe_2$ and $TbCo_2$ compounds for (↑) and (↓) electrons as a function of temperature at a certain value of chemical potential ($\mu = E_F$) were calculated. Fig. 6 (a–d) illustrated the temperature variation of the κ_e/τ. It has been noticed that κ_e/τ for spin-up and spin-down electrons of both compounds increases lineally with increasing the temperature. Therefore, the electronic thermal conductivity for the (↑)(↓) electrons of $TbFe_2$ and $TbCo_2$ is temperature-dependent. To verify that we have calculated κ_e/τ for the (↑)(↓) electrons of $TbFe_2$ and $TbCo_2$ as a function of chemical potential ($\mu - E_F = \pm 0.15$ eV) at three constant temperatures (300, 600 and 900) K. These are shown in Fig. 6(e–h) which show that a significant increases in κ_e/τ occurs with increasing the temperature and the temperature 900 K induced the highest κ_e/τ values, while 300 K induced the lowest κ_e/τ values confirming that 300 k is the optimal temperature which gives the lowest κ_e/τ values in the chemical potential range $\mu - E_F = +0.15$ eV. Therefore, in this chemical potential range the investigated materials expected to give the optimal efficiency.

3.2.3. Seebeck coefficient (thermopower)

We have calculated the Seebeck coefficient or thermopower (S) of $TbFe_2$ and $TbCo_2$ compounds for (↑) and (↓) electrons as a function of temperature at a certain value of chemical potential ($\mu = E_F$) as shown in Fig. 7(a–d). It is clear that the calculated S for the (↑) electrons of $TbFe_2$ represents negative values indicated that the n-type conduction is the dominant, and S significantly increases with increasing the temperature up to 400 K. Above this temperature S exhibit almost stable values around -300 μV/K. Whereas the calculate S for the (↓) electrons of $TbFe_2$ represents $+S$ up to 150 K (i.e. p-type conduction). Rising the temperature above 150 K cause to turn S to negative values which increases with increasing the temperature up to 600 K. Above 600 K $-S$ show stable value around -1120 μV/K. While the calculated S for (↑) electrons of $TbCo_2$ exhibit $-S$ up to 80 K which turn to be positive up to 395 K. Further increase in the temperature leads again to turn S to negative values and reach the maximum value of about -1000 μV/K at 900 K, this observation is in concordance with the experimental measurements [4–6]. We should emphasize that the large S value is attributed to non-zero density of states at E_F.

Furthermore, we have calculated $S$of $TbFe_2$ and $TbCo_2$ for (↑) and (↓) electrons as a function of chemical potential ($\mu - E_F = \pm 0.15$ eV) at three constant temperatures (300, 600 and 900) K as shown in Fig. 7(e–h). One can see in the vicinity of E_F the Seebeck coefficient for (↑) and (↓) electrons of $TbFe_2$ and $TbCo_2$ exhibit several pronounced structures at E_F, below and above E_F, and S represent both n-/p-type conductions along the chemical potential range $\mu - E_F = \pm 0.15$ eV. We would like to highlight that the differences in structure's height and location for (↑) and (↓) electrons of both compounds is attributed to the different values of the non-zero density of states at E_F and the Fermi surface's configuration. It has been found that for (↑) electrons of $TbFe_2$ the highest S values for p-type conductions of about 350 μV/K is achieved at 600 K for $\mu - E_F = -0.017$ eV and for n-type conductions of about -400 μV/K at 900 K for $\mu - E_F = -0.15$ eV. Whereas for (↓) electrons of $TbFe_2$ the highest S for p-type conductions is about 390 μV/K at 900 K for $\mu - E_F = +0.14$ eV, while for n-type conductions is about -353 μV/K at 300 K for $\mu - E_F = -0.08$ eV.

For $TbCo_2$ compound the highest S for (↑) electrons of about 300 μV/K is achieved at 600 K for $\mu - E_F = -0.04$ eV, and at 600 K and 900 K at $\mu - E_F = +0.09$ eV for p-type conductions, while for n-type conductions it is about -430 μV/K at 900 K for

Fig. 2. (a) Calculated Fermi surface for (↑) electrons of $TbFe_2$ the white regions represent the hole concentration while the colored regions correspond to the presence of electrons. The red color represent the highest speed, yellow green and blue have intermediate speed whereas the violet color show lowest speed; (b) calculated spin-up electronic band structure of $TbFe_2$ compound along with the calculated carriers concentration as a function of chemical potential ($\mu - E_F = \pm 0.2$ eV) at three constant temperatures (300, 600 and 900) K for spin-up electrons of $TbFe_2$ compound; (c) Calculated Fermi surface for (↓) electrons of $TbFe_2$ the white regions represent the hole concentration while the colored regions correspond to the presence of electrons. The red color represent the highest speed, yellow green and blue have intermediate speed whereas the violet color show lowest speed; (d) calculated spin-down electronic band structure of $TbFe_2$ compound along with the calculated carriers concentration as a function of chemical potential ($\mu - E_F = \pm 0.2$ eV) at three constant temperatures (300, 600 and 900) K for spin-down electrons of $TbFe_2$ compound; (e) Calculated Fermi surface for (↑) electrons of $TbCo_2$ the white regions represent the hole concentration while the colored regions correspond to the presence of electrons. The red color represent the highest speed, yellow green and blue have intermediate speed whereas the violet color show lowest speed; (f) calculated spin-up electronic band structure of $TbCo_2$ compound along with the calculated carriers concentration as a function of chemical potential ($\mu - E_F = \pm 0.2$ eV) at three constant temperatures (300, 600 and 900) K for spin-up electrons of $TbCo_2$compound; (g) Calculated Fermi surface for (↓) electrons of $TbCo_2$ the white regions represent the hole concentration while the colored regions correspond to the presence of electrons. The red color represent the highest speed, yellow green and blue have intermediate speed whereas the violet color show lowest speed; (h) calculated spin-down electronic band structure of $TbCo_2$ compound along with the calculated carriers concentration as a function of chemical potential ($\mu - E_F = \pm 0.2$ eV) at three constant temperatures (300, 600 and 900) K for spin-down electrons of $TbCo_2$ compound; We would like to mention that the colors in the electronic band structures means nothing just to illustrated the bands in clear way. (For interpretation of the references to color in this figure legend, the reader is referred to the web version of this article.)

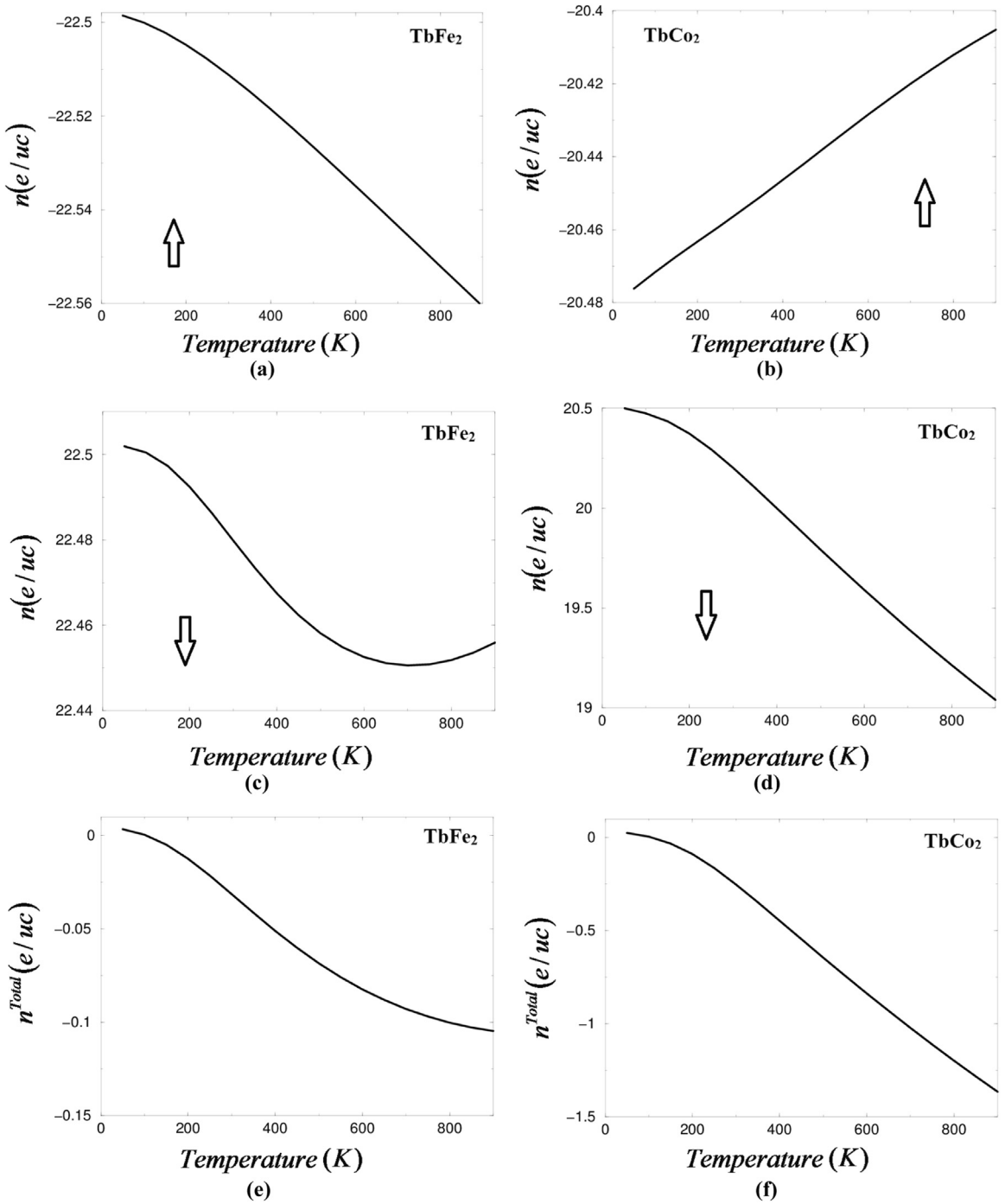

Fig. 3. (a, b) The temperature induced carrier concentration per unit cell (e/uc) for spin-up electrons versus temperature for $TbFe_2$ and $TbCo_2$ compounds; (c, d) The temperature induced carrier concentration per unit cell (e/uc) for spin-down electrons versus temperature for $TbFe_2$ and $TbCo_2$ compounds; (e-f) The temperature induced total carrier concentration per unit cell (e/uc) versus temperature for $TbFe_2$ and $TbCo_2$ compounds.

$\mu - E_F = -0.02$ eV. The largest S for (↓) electrons are 770 μV/K at 900 k for $\mu - E_F = -0.02$ eV for the p-type conductions, while for n-type conductions it is about −630 μV/K at 900 K for $\mu - E_F = +0.09$ eV.

It has been found that the total S of $TbCo_2$ is larger than that of $TbFe_2$. That is attributed to the fact that the DOS at E_F and the valence electrons in $TbCo_2$ are higher than that in $TbFe_2$. For an increase of the valence electrons the absolute value of S is decreased. This is explained by the increase of the electron concentration in the bands. By increasing the number of valence electrons additional electrons are added to the d band at the Fermi energy [30]. This leads to an increase of the carrier concentration (n). The increase of n leads to a decrease of S [27]. The interrelationship between n and S can be seen from relatively simple models of electron transport. For simple metals or degenerate semiconductors with parabolic bands and energy independent scattering the S is given by;

$$S = \frac{8\pi^2 k_B^2}{3eh^2} m^* T \left(\frac{\pi}{3n}\right)^{3/2} \quad (2)$$

where n is the carrier concentration and m^* is the effective mass of the carrier. It can be clearly seen that S depends on the n and on the effective mass m^*. The latter depend on the shape of the bands.

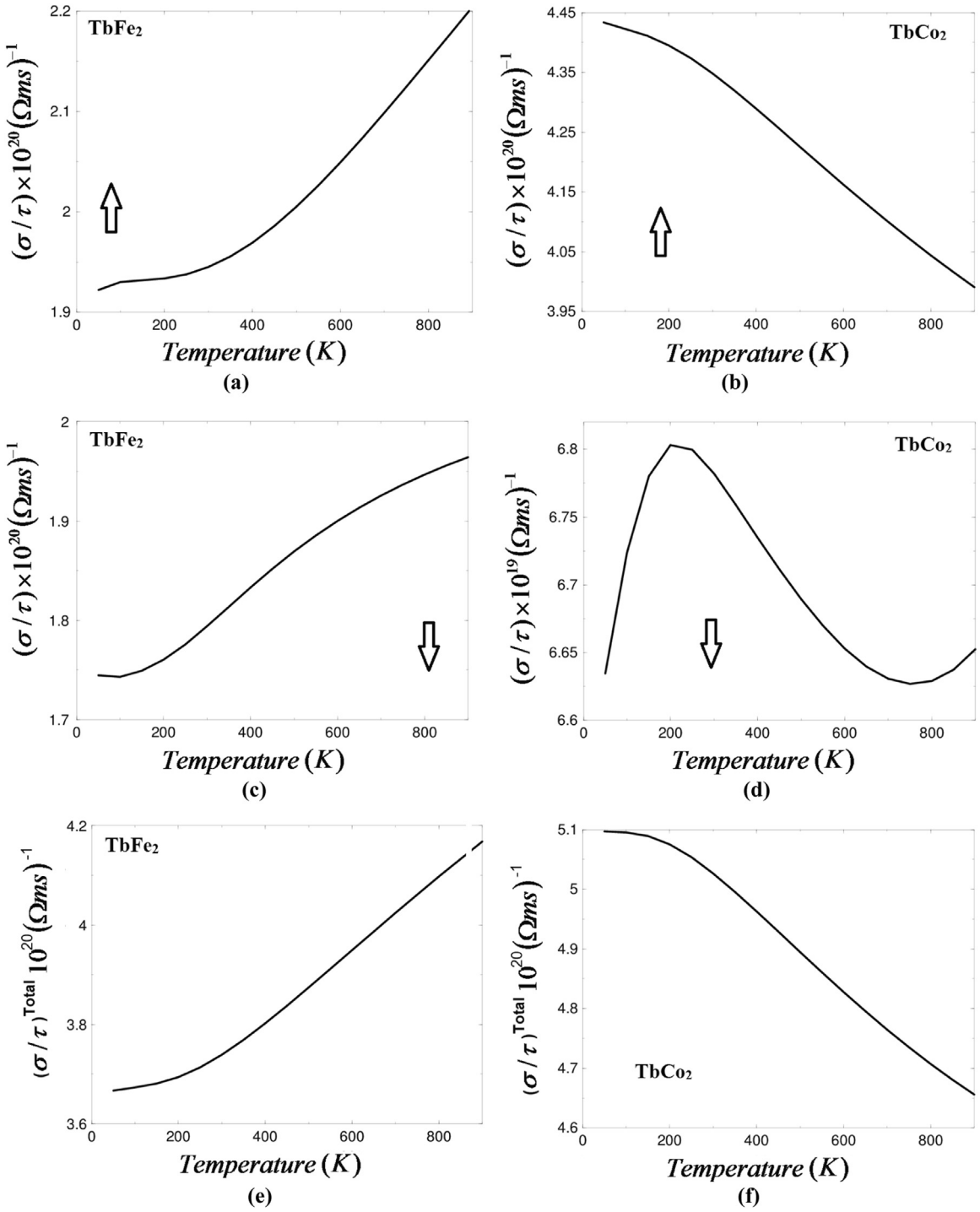

Fig. 4. (a, b) The electrical conductivity for spin-up electrons versus temperature for $TbFe_2$ and $TbCo_2$ compounds; (c, d) The electrical conductivity for spin-down electrons versus temperature for $TbFe_2$ and $TbCo_2$ compounds; (e, f) The total electrical conductivity versus temperature for $TbFe_2$ and $TbCo_2$ compounds.

Following Fig. 7(e–h) it is clear that the obtained values of S are negative / positive for the entire range of the chemical potential suggesting the presence of n/p-type charge carriers. The sign of S indicates the type of dominant charge carriers, S with positive sign represent the p-type materials, whereas n-type materials have negative S [16,25,31,32]. We should emphasize that the temperature has significant influence on S along the chemical potential range $\mu - E_F = \pm 0.15$ eV. The Seebeck coefficient is an important quantity which is related to the electronic band structure of the materials.

3.2.4. Power factor (P)

Usually the power factor (P) defined as (electrical conductivity times the square of Seebeck coefficient), thus P is directly proportional to S^2 and σ/τ. To gain high P therefore, the S^2 and σ/τ values needs to be maintained. As P comes in the numerator of the dimensionless figure of merit ($ZT = S^2\sigma T/k_e + k_l$) [26,33] therefore, P is an important quantity which play principle role in evaluating the transport properties of the materials. Fig. 8(a–d) illustrated the calculated P for (↑) and (↓) electrons of $TbFe_2$ and $TbCo_2$ as a function of chemical potential $\mu - E_F = \pm 0.15$ eV at three fixed

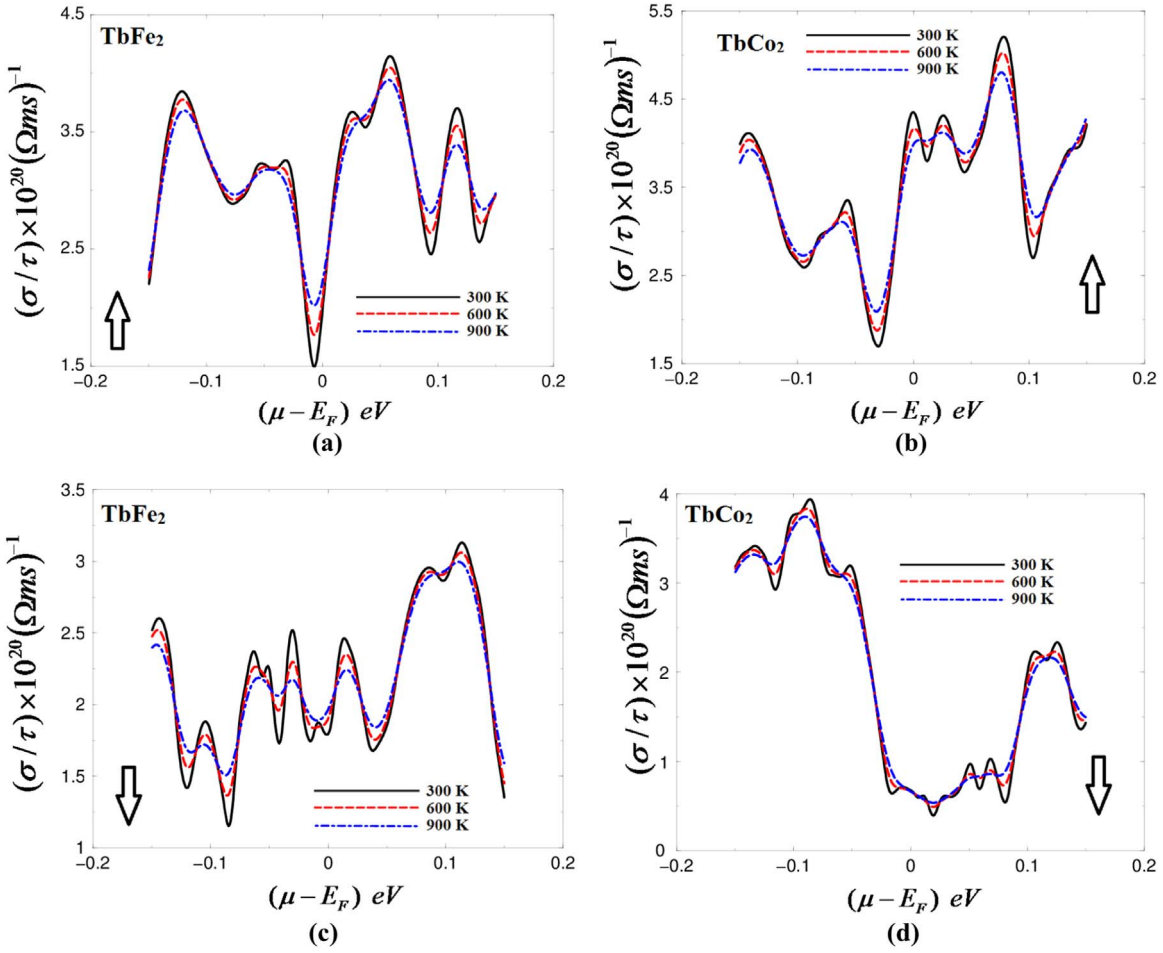

Fig. 5. (a,b) The electrical conductivity of $TbFe_2$ and $TbCo_2$ for spin-up electrons as a function of chemical potential ($\mu - E_F = \pm 0.15$ eV) at three constant temperatures (300, 600 and 900) K; (c,d) The electrical conductivity of $TbFe_2$ and $TbCo_2$ for spin-down electrons as a function of chemical potential ($\mu - E_F = \pm 0.15$ eV) at three constant temperatures (300, 600 and 900) K.

temperatures (300, 600 and 900) K. For (↑) electrons of $TbFe_2$, the highest P value of about $3.75\times10^{11}\left(W/mk^2s\right)$ is achieved at 900 K for $\mu - E_F = -0.14$ eV, $2.77\times10^{11}\left(W/mk^2s\right)$ is achieved at 600 K for $\mu - E_F = -0.017$ eV and $1.44\times10^{11}\left(W/mk^2s\right)$ is achieved at 300 K for $\mu - E_F = -0.014$ eV and $\mu - E_F = -0.001$ eV. Whereas the (↓) electrons of $TbFe_2$, show the highest value of about $3.05\times10^{11}\left(W/mk^2s\right)$ at 900 K and $2.31\times10^{11}\left(W/mk^2s\right)$ at 600 K for $\mu - E_F = 0.14$ eV, while it is $1.79\times10^{11}\left(W/mk^2s\right)$ at 300 K for $\mu - E_F = -0.08$ eV. For (↑) electrons of $TbCo_2$, the highest P value of about $5.13\times10^{11}\left(W/mk^2s\right)$ is achieved at 900 K and $2.23\times10^{11}\left(W/mk^2s\right)$ is achieved at 600 K for $\mu - E_F = -0.015$ eV, while for 300 K it is about $2.08\times10^{11}\left(W/mk^2s\right)$ for $\mu - E_F = +0.092$ eV. Whereas the (↓) electrons of $TbCo_2$, show the highest value of about $7.73\times10^{11}\left(W/mk^2s\right)$ at 900 K and $5.3\times10^{11}\left(W/mk^2s\right)$ at 600 K for $\mu - E_F = -0.027$ eV, while it is $2.4\times10^{11}\left(W/mk^2s\right)$ at 300 K for $\mu - E_F = +0.08$ eV.

It is clear that the power factor of $TbCo_2$ compound is higher than that of $TbFe_2$ compound that is attributed to the fact the total S of $TbCo_2$ is larger than that of $TbFe_2$ which is returned to the fact that the DOS at E_F and the valence electrons in $TbCo_2$ are more than that in $TbFe_2$.

We would like to mention here in our previous works [34–37] we have calculated the transport properties using FPLAPW method within BoltzTraP code on several systems whose transport properties are known experimentally, in those previous calculations we found very good agreement with the experimental data. Thus, we believe that our calculations reported in this paper would produce very accurate and reliable results.

4. Conclusions

The transport properties for the spin-up and spin-down electrons of the Laves phase $TbFe_2$ and $TbCo_2$ compounds were performed based on the rigid band approach and the semi-classical Boltzmann theory as incorporated within BoltzTraP code. The calculated spin-polarized electronic band structure and the density of states reveal the metallic nature of these compounds with different density of states at E_F for the spin-up and spin-down electrons, which leads to unusual transport properties because the (↑) and (↓) densities contributes to the states at E_F. Moreover, $TbFe_2$ and $TbCo_2$ compounds possess parabolic bands in the vicinity of Fermi level therefore, the carriers exhibit low effective mass and hence high mobility. It has been found that the transport coefficients increases/reduces with increasing the temperature therefore, the spin-up/down transport coefficients are temperature-dependent. It has been found that the total S of $TbCo_2$ is larger than that of $TbFe_2$. That is attributed to the fact that the DOS at E_F and the valence electrons in $TbCo_2$ are more than that in $TbFe_2$. The increase of the Seebeck coefficient also leads to a

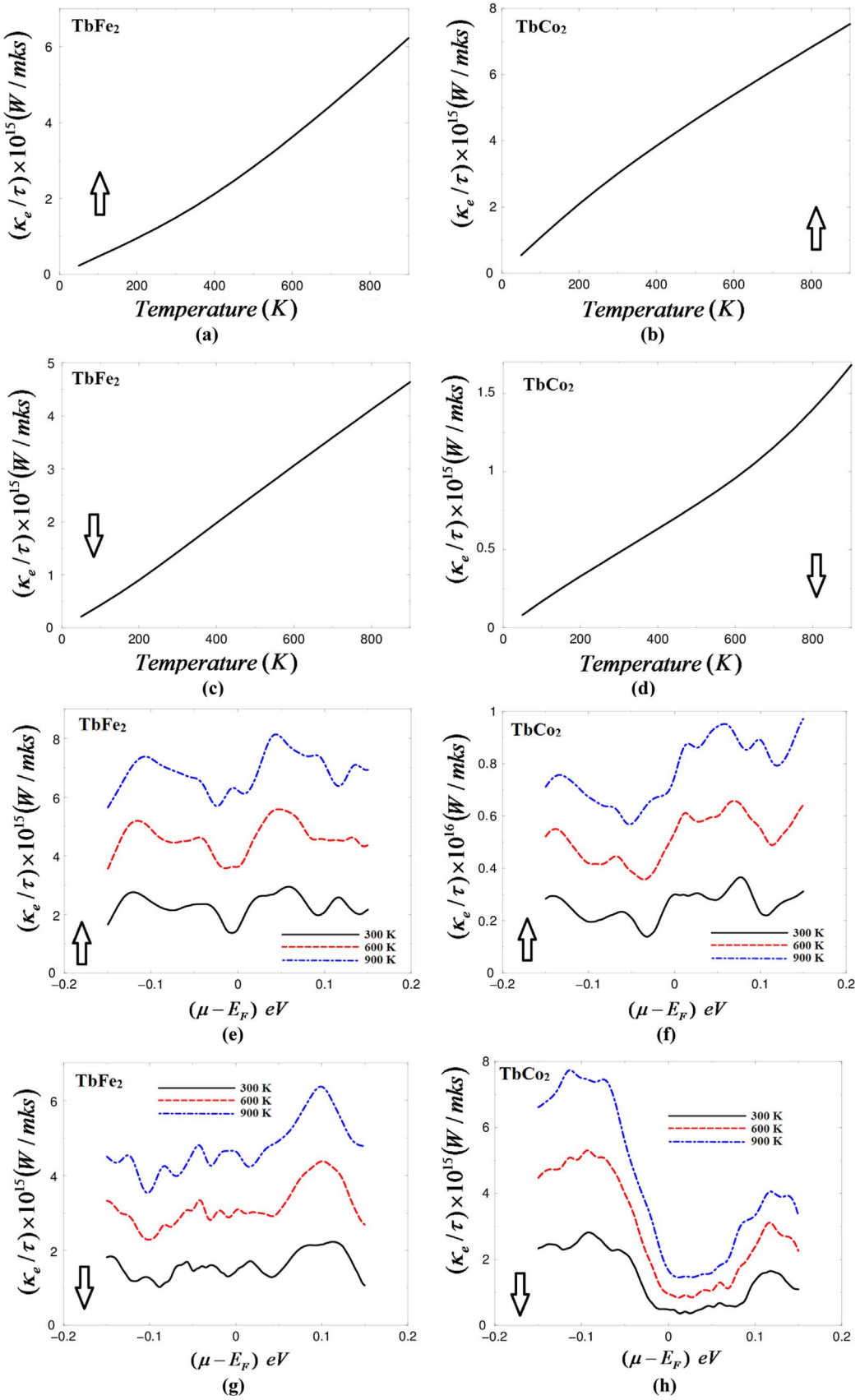

Fig. 6. (a, b) The electronic thermal conductivity for spin-up electrons versus temperature for $TbFe_2$ and $TbCo_2$ compounds; (c, d) The electronic thermal conductivity for spin-down electrons versus temperature for $TbFe_2$ and $TbCo_2$ compounds; (e, f) The electronic thermal conductivity of $TbFe_2$ and $TbCo_2$ for spin-up electrons as a function of chemical potential ($\mu - E_F = \pm 0.15$ eV) at three constant temperatures (300, 600 and 900) K; (g, h) The electronic thermal conductivity of $TbFe_2$ and $TbCo_2$ for spin-down electrons as a function of chemical potential ($\mu - E_F = \pm 0.15$ eV) at three constant temperatures (300, 600 and 900) K.

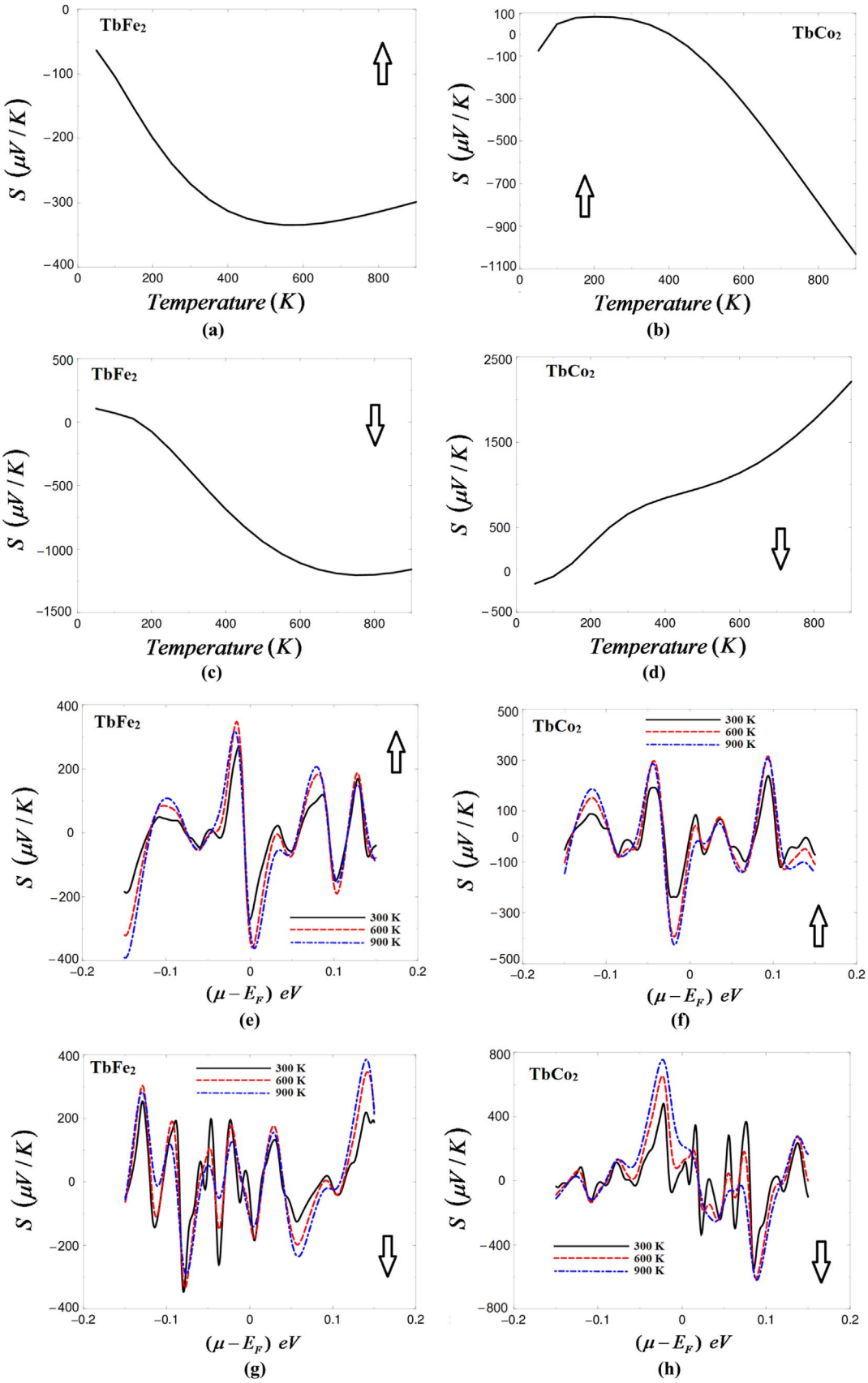

Fig. 7. (a, b) The Seebeck coefficient for spin-up electrons versus temperature for $TbFe_2$ and $TbCo_2$ compounds; (c, d) The Seebeck coefficient for spin-down electrons versus temperature for $TbFe_2$ and $TbCo_2$ compounds; (e, f) The Seebeck coefficient of $TbFe_2$ and $TbCo_2$ for spin-up electrons as a function of chemical potential ($\mu - E_F = \pm 0.15$ eV) at three constant temperatures (300, 600 and 900) K; (g, h) The Seebeck coefficient of $TbFe_2$ and $TbCo_2$ for spin-down electrons as a function of chemical potential ($\mu - E_F = \pm 0.15$ eV) at three constant temperatures (300, 600 and 900) K.

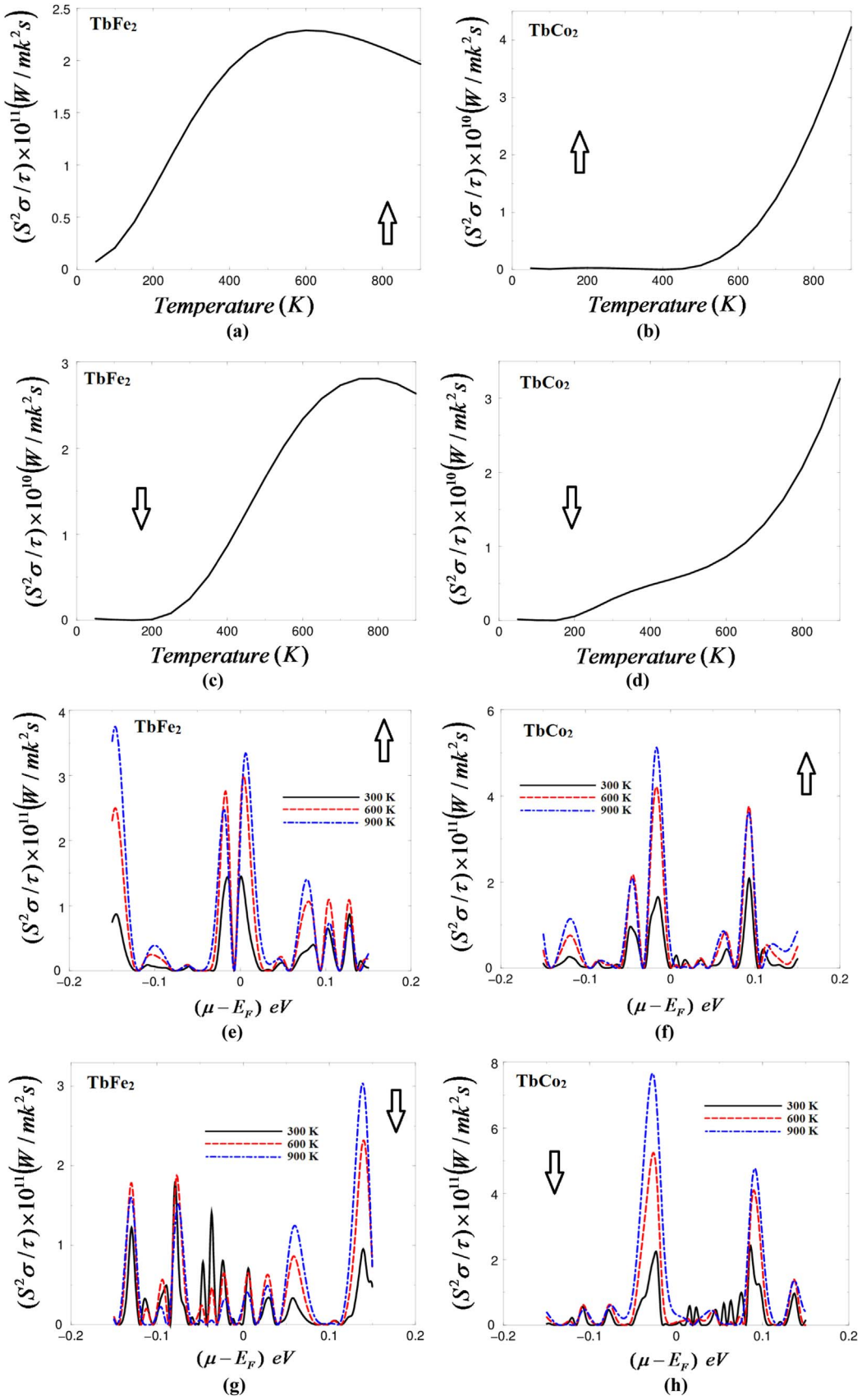

Fig. 8. (a, b) The power factor for spin-up electrons versus temperature for $TbFe_2$ and $TbCo_2$ compounds; (c, d) The power factor for spin-down electrons versus temperature for $TbFe_2$ and $TbCo_2$ compounds; (e, f) The power factor of $TbFe_2$ and $TbCo_2$ for spin-up electrons as a function of chemical potential ($\mu - E_F = \pm 0.15$ eV) at three constant temperatures (300, 600 and 900) K; (g, h) The power factor of $TbFe_2$ and $TbCo_2$ for spin-down electrons as a function of chemical potential ($\mu - E_F = \pm 0.15$ eV) at three constant temperatures (300, 600 and 900) K.

maximum of the power factor. Therefore, the power factor of $TbCo_2$ is higher than that of $TbFe_2$. This makes them attractive candidates for materials used in spin voltage generators. We would like to mentioned that the calculated Seebeck coefficient of $TbCo_2$ in concordance with the available experimental data.

Some important notes

We have used η as symbol for the mobility in order to distinguish it from the chemical potential μ.

Acknowledgments

The result was developed within the CENTEM project, reg. no. CZ.1.05/2.1.00/03.0088, cofunded by the ERDF as part of the Ministry of Education, Youth and Sports OP RDI program and, in the follow-up sustainability stage, supported through CENTEM PLUS (LO1402) by financial means from the Ministry of Education, Youth and Sports under the "National Sustainability Program I. Computational resources were provided by MetaCentrum (LM2010005) and CERIT-SC (CZ.1.05/3.2.00/08.0144) infrastructures.

References

[1] S. Khmelevskyi, P. Mohn, J. Phys.: Condens. Matter 12 (2000) 9453–9464.
[2] E. Gratz, A.S. Markosyan, J. Phys.: Condens. Matter 13 (2001) R385–R413.
[3] Satoshi Hirosawa, Yoji Nakamura, J. Magn. Magn. Mater. 25 (1982) 284–294.
[4] E. Gratz, H. Sassik, H. Nowotny, J. Phys. F: Met. Phys. 11 (1981) 429–435.
[5] M. Cyrot, M. Lavagna, J. Phy. 40 (1979) 763.
[6] E. Gratz, A.S. Markosyan, J. Phys.: Condens. Matter 13 (2001) 385.
[7] B.L. Ahuja, H.S. Mund, Jagrati Sahariya, Alpa Dashora, Madhumita Halder, S. M. Yusuf, M. Itou, Y. Sakurai, J. Alloy. Compd. 633 (2015) 430–434.
[8] J.J. Rhyne, N.C. Koon, H.A. Alperin, Magnetic Excitations in $TbFe_2$, pp 313–314, Isbn: 978-1-4613-3056-1 (Print) 978-1-4613-3054-7 (Online).
[9] F. Hellman, A.L. Shapiro, E.N. Abarra, R.A. Robinson, R.P. Hjelm, P.A. Seeger, J. J. Rhyne, J.I. Suzuki, Phys. Rev. B 59 (1999) 11408.
[10] P. Blaha, K. Schwarz, G.K.H. Madsen, D. Kvasnicka, J. Luitz, WIEN2k, An Augmented Plane Wave Plus Local Orbitals Program for Calculating Crystal Properties, Vienna University of Technology, Austria, 2001.
[11] J.P. Perdew, S. Burke, M. Ernzerhof, Phys. Rev. Lett. 77 (1996) 3865.
[12] V.I. Anisimov, I.V. Solvyev, M.A. Korotin, M.T. Czyzyk, C.A. Sawatzky, Phys. Rev. B 48 (1993) 16929.
[13] A.I. Liechtenstein, V.I. Anisimov, Zaanen, J. Phys. Rev. B 52 (1995), R5467.
[14] O.K. Andersen, Phys. Rev. B 12 (1975) 3060.
[15] J.P. Perdew, Y. Wang, Phys. Rev. B 45 (1992) 13244.
[16] G.K.H. Madsen, D.J. Singh, Comput. Phys. Commun. 175 (2006) 67–71.
[17] P.B. Allen, in: J.R. Chelikowsky, S.G. Louie (Eds.), Quantum Theory of Real Materials, Kluwer, Boston, 1996, pp. 219–250.
[18] J.M. Ziman, Electrons and Phonons, Clarendon, Oxford, 2001.
[19] C.M. Hurd, The Hall Effect in Metals and Alloys, Plenum, New York, 1972.
[20] H.S. Saini, M. Singh, A.H. Reshak, M.K. Kashyap, J. Magn. Magn. Mater. 331 (2013) 1–6.
[21] Y. Saeed, S. Nazir, A. Shaukat, A.H. Reshak, J. Magn. Magn. Mater. 322 (2010) 3214–3222.
[22] R.I. Eglitis, G. Borstel, Phys. Status Solidi A 202 (2005) R13–R15.
[23] R.I. Eglitis, Phys. Scr. 90 (2015) 094012.
[24] J. Kübler, A.R. Williams, C.B. Sommers, Phys. Rev. B 28 (1983) 1745.
[25] S. Sharma, S.K. Pandey, J. Phys.: Condens. Matter 26 (2014) 215501.
[26] A.H. Reshak, S. Azam, J. Magn. Magn. Mater. 342 (2013) 80–86.
[27] G.J. Snyder, E.S. Toberer, Nat. Mater. 7 (2008) 105–114.
[28] H.J. Xiang, D.J. Singh, Phys. Rev. B 76 (2007) 195111.
[29] A.S. Botana, P.M. Botta, C. Calle, A. de la, Pineiro, V. Pardo, D. Baldomir, J. A. Alonso, Phys. Rev. B 83 (2011) 184420.
[30] S. Ouardi, B. Balke, A. Gloskovskii, G.H. Fecher, C. Felser, G. Schönhense, T. Ishikawa, T. Uemura, M. Yamamoto, H. Sukegawa, W. Wang, K. Inomata, Y. Yamashita, H. Yoshikawa, S. Ueda, K. Kobayashi, J. Phys. D: Appl. Phys. 42 (2009) 084010.
[31] B. Xu, X. Li, G. Yu, J. Zhang, S. Ma, Y. Wang, L. Yi, J. Alloy. Compd. 565 (2013) 22–28.
[32] T.J. Scheidemantel, C. Ambrosch-Draxl, T. Thonhauser, J.V. Badding, J.O. Sofo, Phys. Rev. B 68 (125210) (2003) 6.
[33] Chenming Calvin Hu, Modern semiconductor devices for integrated circuits, Part I: Electrons and Holes in a Semiconductor November 11, 2011.
[34] A.H. Reshak, S. Auluck, Comput. Mater. Sci. 96 (2015) 90–95.
[35] A.H. Reshak, J. Phys. Chem. Solids 78 (2015) 46–52.
[36] A.H. Reshak, Renew. Energy 76 (2015) 36–44.
[37] (a) A.H. Reshak, RSC Adv. 4 (2014) 63137;
(b) A.H. Reshak, RSC Adv. 5 (2015) 47569.